Comparison of Cascaded and Flatness-Based Control of a Pneumatically-Driven Rotary Joint

Kathrin Hoffmann[1], Christian Trapp[2], Alexander Hildebrandt[2], and Oliver Sawodny[1]

***Abstract*— When it comes to robot joints, pneumatic actuators are an interesting alternative to classic electric actuators. They are inherently compliant due to the compressibility of air, which is an advantageous safety feature for human-machine collaboration. In this work, we consider a recently developed pneumatic swivel drive, to be employed as a robot rotary joint. This joint exhibits strong nonlinearities, which makes it challenging to design a trajectory tracking controller. We formulate the nonlinear multiple input multiple output (MIMO) model of the joint's kinetics and pressure dynamics. Based thereon, two model-based nonlinear control concepts are presented. The first one is a cascaded controller consisting of an outer loop with a joint angle controller and disturbance observer, and an inner pressure control loop. For the second concept, differential flatness of the system is shown and a flatness-based controller is derived, which combines both kinetics and pressure dynamics in one central controller. Experimental results demonstrate the trajectory tracking performance of both controllers. Based on these results, the differences between the two control strategies are analyzed. This provides the foundation for the control of more complex pneumatically-driven robot manipulators.**

I. INTRODUCTION

Pneumatic drives are commonly used in automation for handling tasks. They are characterized by a high power-to-weight ratio and low cost, which also makes them an interesting candidate for robotic applications. Another property of pneumatic drives is the compressibility of air, so that these actuators are inherently compliant, which is an advantageous safety feature for human-machine collaboration. Moreover, they are direct drives without gears, which distinguishes them from most electric drives. The absence of a gear reduces the inertia, and, therefore, the acting torque in case of a collision, thus, increasing safety.

While pneumatic actuators in industrial applications are mostly linear drives or pneumatic muscles [1], typical collaborative robot kinematics require rotational drives. Researchers have, for example, developed a conversion between linear and rotational motion [2] or soft fluidic rotary actuators [3]. Recently, improvements in drive design and especially valve hardware made it possible to employ pneumatic swivel drives as robot joints, as it is done in this research.

Pneumatic drives generally exhibit highly nonlinear behavior [4], resulting from the compressibility of air, friction in the seal between moving and static components, as well as from nonlinear valve characteristics. Therefore, the controller design has to account for such nonlinearities. Moreover, the pressure dynamics in the pneumatic subsystem are not negligibly fast compared to the mechanical subsystem, so that the actuation cannot be considered to be infinitely fast, as it is the case in electric drives.

Previous works on the control of pneumatic actuators found that with nonlinear control based on exact linearziation, a better tracking performance can be achieved than with linear control laws [5], [6]. The latter papers deal with in-line drives controlled as single input single output systems, for which the computational complexity is still low, whereas in our case the rotary drive is of multiple input multiple output (MIMO) type. More complex pneumatic robots are usually controlled by a cascaded controller consisting of two separate nonlinear controllers for mechanics and pressure dynamics [7], [8].

In this work, we present two model-based nonlinear control concepts for the above introduced robot joint. The first one is a cascaded controller consisting of an outer joint angle controller and an inner pressure controller. An additional disturbance observer (DOB) with integrating behavior estimates disturbance torques, which are then compensated. The second control concept is based on the differential flatness of the system and comprises both kinetics and pressure dynamics in one central controller. The differential flatness property is shown, and the controller that linearizes the system exactly by static feedback is derived. Moreover, for the central controller, a stabilizing feedback as well as feedforward for trajectory tracking and friction compensation are designed. These controllers are implemented on the robot joint and their performance is demonstrated in experiments. Beyond that, the experimental results are compared and the differences resulting from the respective control structures are pointed out, which has not yet been done in the literature on the individual control concepts.

This paper is organized as follows: The mechanical and pneumatic model of the joint are derived in Section II. In Section III, first a cascaded and second a flatness-based controller are designed. These controllers are applied to the presented actuator in Section IV, in which the experimental results are shown. Finally, we compare the results from the two control approaches and give a conclusion.

II. SYSTEM MODEL

In this section, the dynamic model of the pneumatically-driven rotational actuator is derived. This actuator, depicted in Fig. 1, consists of two pressure chambers separated by a movable swivel wing and a static chamber seal. The pressure

[1]Kathrin Hoffmann and Oliver Sawodny are with Institute for System Dynamics, University of Stuttgart, D-70563 Stuttgart, Germany {kathrin.hoffmann, sawodny}@isys.uni-stuttgart.de

[2]Christian Trapp and Alexander Hildebrandt are with Robotics System Design, Festo SE & Co. KG, D-73734 Esslingen, Germany

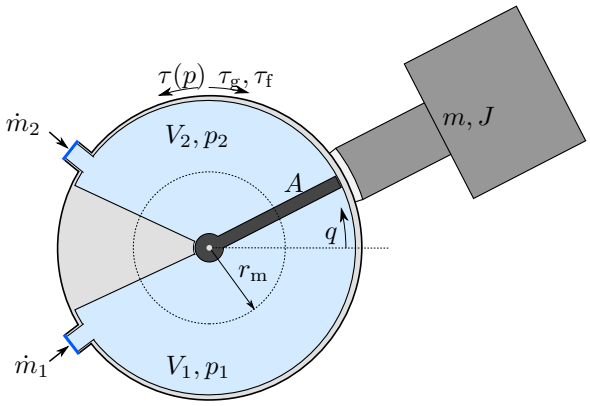

Fig. 1. Hardware setup.

of each chamber can be controlled individually and a pressure difference generates the torque $\tau(\boldsymbol{p}) = A r_\mathrm{m}(p_1 - p_2)$ with A being the effective area and r_m the effective radius of the swivel wing. The air mass flow to and from each chamber is controlled by separate valves, so that the overall system is of MIMO type.

A. Mechanical Model

The joint is mounted such that its rotation axis and center position $q = 0$ are horizontal, see Fig. 1. A payload of mass m and inertia J is attached eccentrically to the joint's shaft with r_cog being the lever arm of the center of gravity with respect to the rotation axis, leading to a gravitational torque $\tau_\mathrm{g} = m\, g\, r_\mathrm{cog} \cos(q)$. The equation of motion reads

$$J\ddot{q} + \tau_\mathrm{g} = \tau(\boldsymbol{p}) - \tau_\mathrm{f}. \tag{1}$$

The friction model contains Coulomb and viscous friction

$$\tau_\mathrm{f} = f_\mathrm{c} \tanh\left(\frac{\dot{q}}{\dot{q}_\mathrm{c}}\right) + f_\mathrm{v}\dot{q}, \tag{2}$$

where f_c is the Coulomb friction torque and f_v is the viscous friction coefficient. Using the $\tanh$ function with velocity threshold $\dot{q}_\mathrm{c}$, it is continuous around $\dot{q} = 0$ to avoid chattering.

B. Pneumatic Model

The pressure p_i in each chamber $i \in \{1, 2\}$ is controlled by a mass flow $\dot{m}_i$. This mass flow of each chamber is set by two valves, one for pressurizing and one for exhaust. The pneumatic model of each chamber is based on the first law of thermodynamics for open systems and the air is assumed to be an ideal gas. It undergoes a polytropic process [4], [9]

$$\dot{p}_i = \frac{n}{V_i(q)}\left(RT\dot{m}_i - \dot{V}_i(\dot{q})\, p_i\right) \tag{3}$$

with polytropic index n, specific gas constant R, temperature T, and chamber volume $V_i(q)$. Since the valves are attached to the rotary drive, the tubes are short and tube effects in between are neglected.

Each valve is modeled as a nozzle according to ISO 6358 [10], in which the flow is characterized by the two parameters sonic conductance C and critical pressure ratio b, which are determined experimentally. The mass flow depends on the pressures before the valve p_prim and behind the valve p_sec as well as the density of air ρ and reads

$$\dot{m} = C_\mathrm{max} C_\mathrm{rel}(\nu_\mathrm{valve})\, p_\mathrm{prim} \rho \Psi\left(b, \frac{p_\mathrm{sec}}{p_\mathrm{prim}}\right), \tag{4}$$

where the sonic conductance is normalized by its maxiumum value to the relative conductance C_rel. Equation (4) also depends on the flow function Ψ [10], which is defined as

$$\Psi(b, \beta) = \begin{cases} 1 & \beta < b \\ \sqrt{1 - \left(\frac{\beta - b}{1 - b}\right)^2} & \beta \geq b \end{cases} \tag{5}$$

with pressure ratio $\beta = p_\mathrm{sec}/p_\mathrm{prim}$. The valve relative conductance C_rel, as a measure of valve opening degree, in turn is a nonlinear function of the valve input voltage ν_valve and has to be identified experimentally [9].

III. CONTROL

For the presented actuator, we design two different control laws, a cascaded one described in Section III-B and a flatness-based one in Section III-C, and compare their performance afterwards in order to analyze the physical implications of their structural differences. Despite these differences, both control laws require the same compensation of the nonlinearities (4), (5) resulting from the valve characteristics. Therefore, the inversion of the valve model is separated from the rest of the feedback controller design and is outlined in the first of the following subsections. Based thereon, in the consecutive subsections, we consider the mass flows to and from the pressure chambers as the control input $\boldsymbol{u} = [\dot{m}_1,\ \dot{m}_2]^T$. The measured outputs are the angle q and the chamber pressures p_1, p_2.

A. Mass Flow Control

The nonlinearities resulting from the valve are compensated in two steps by model inversion. First, the desired relative conductance is computed by an inversion of the mass flow equation (4) as

$$C_\mathrm{rel,d} = \frac{\dot{m}_\mathrm{d}}{C_\mathrm{max} p_\mathrm{prim} \rho \Psi(b, p_\mathrm{sec}/p_\mathrm{prim})}. \tag{6}$$

Second, the relative conductance characteristic curve is inverted numerically to arrive at the desired voltage input $\nu_\mathrm{valve} = C_\mathrm{rel}^{-1}(C_\mathrm{rel,d})$ to the valve. In order to improve mass flow accuracy and compensate for leakage, a mass flow DOB is implemented, but details on its design are outside of the scope of this paper.

B. Cascaded Controller

The cascaded controller, as depicted in Fig. 2, consists of an inner pressure control loop and an outer joint angle control loop for path tracking.

The **outer loop** is designed as a computed torque controller [11]

$$\tau_\mathrm{d}(\boldsymbol{p}) = J\nu_\mathrm{mech} + \tau_\mathrm{g} + \tau_\mathrm{f} \tag{7}$$

including gravitational compensation and friction feedforward control. In order to track reference trajectories $q(t) \rightarrow q_{\mathrm{d}}(t)$, the new input

$$\nu_{\mathrm{mech}} = \ddot{q}_{\mathrm{d}} + c_1(\dot{q} - \dot{q}_{\mathrm{d}}) + c_2(q - q_{\mathrm{d}}) \tag{8}$$

consists of a PD-feedback and a feedforward controller. The dynamics of the tracking error $e(t) = q_{\mathrm{d}}(t) - q(t)$ have to be asymptotically stable by an appropriate choice of coefficients c_i. We choose the feedback gains $c_1 = 2d\omega$ and $c_2 = \omega^2$, which render the error dynamics a second order system with eigenfrequency ω and damping d.

In order to estimate disturbance torques, which result for example from model uncertainties or unmodeled friction effects, we design a torque **disturbance observer** (DOB). It is a Luenberger type observer with model

$$\hat{\boldsymbol{x}} = \begin{bmatrix} \hat{q} & \dot{\hat{q}} & \hat{\tau}_{\mathrm{dist}} \end{bmatrix}^T \tag{9a}$$

$$\dot{\hat{\boldsymbol{x}}} = \begin{bmatrix} 0 & 1 & 0 \\ 0 & 0 & -\frac{1}{J} \\ 0 & 0 & 0 \end{bmatrix} \hat{\boldsymbol{x}} + \begin{bmatrix} 0 \\ \frac{Ar_{\mathrm{m}}}{J} \\ 0 \end{bmatrix} (p_1 - p_2) + \boldsymbol{L}\,(q - \hat{q})\,. \tag{9b}$$

We choose the dynamics of the estimation error $(q - \hat{q})$ as a series interconnection of a PT_2 and PT_1 system with identical corner frequency. This yields the observer gain $\boldsymbol{L} = [\omega_{\mathrm{obs}}(2d_{\mathrm{obs}} + 1),\ \omega_{\mathrm{obs}}^2(2d_{\mathrm{obs}} + 1),\ \omega_{\mathrm{obs}}^3]^T$. This tuning approach for 3rd order error dynamics, which was introduced by [9], provides a both well-performing and physically interpretable result, so that the observer rate of convergence can be tuned in conjunction with the corner frequency of the controller. In the cascaded control structure, the estimated disturbance torque $\hat{\tau}_{\mathrm{dist}}$ is then compensated in addition to (7). The present observer has integrating behavior with respct to the estimation error $(q - \hat{q})$.

In the next step, the desired torque $\tau_{\mathrm{d}}(p)$ is converted to the desired chamber pressures

$$p_{\{1,2\},\mathrm{d}} = p_{\mathrm{m,d}} \pm \frac{\tau_{\mathrm{d}}}{2Ar_{\mathrm{m}}}, \tag{10}$$

in which the desired mean pressure p_{m} provides an additional degree of freedom.

In the **inner loop**, we control the pressure of each chamber by exact I/O linearization [12]. To this end, (3) is exactly linearized by

$$\dot{m}_{i,\mathrm{d}} = \frac{1}{RT}\left(\frac{V_i(q)}{n}\nu_i + \dot{V}_i(\dot{q})\,p_i\right) \tag{11}$$

and as virtual input ν_i, we apply a proportional controller with feedforward

$$\nu_i = \dot{p}_{i,\mathrm{d}} + K\,(p_{i,\mathrm{d}} - p_i)\,. \tag{12}$$

For $\dot{p}_{i,\mathrm{d}}$, we introduce a flatness-based central feedforward control. As described in Section III-C, the overall actuator is a differentially flat system, so that one central feedforward controller for both the mechanical and pneumatic subsystem can be computed from the reference trajectory. With this approach, the feedforward path of the cascaded controller is equivalent to a flatness-based feedforward linearization.

C. Flatness-Based Controller

The mechanics and pressure dynamics constitute a nonlinear input affine MIMO system

$$\dot{\boldsymbol{x}} = \boldsymbol{f}(\boldsymbol{x}) + \sum_{i=1}^{2} \boldsymbol{g}_i(\boldsymbol{x})\,u_i. \quad \boldsymbol{x}(0) = \boldsymbol{x}_0 \tag{13}$$

with state $\boldsymbol{x} = \begin{bmatrix} q,\ \dot{q},\ p_1,\ p_2 \end{bmatrix}^T$ and input $\boldsymbol{u} = [\dot{m}_1,\ \dot{m}_2]^T$. The vector fields are

$$f(\boldsymbol{x}) = \begin{bmatrix} x_2 \\ \frac{1}{J}\left(-mgr_{\mathrm{cog}}\cos(x_1) + Ar_{\mathrm{m}}\,(x_3 - x_4) - \tau_{\mathrm{f}}(x_2)\right) \\ \frac{-nx_3\dot{V}_1(x_2)}{V_1(x_1)} \\ \frac{-nx_4\dot{V}_2(x_2)}{V_2(x_1)} \end{bmatrix} \tag{14}$$

$$\boldsymbol{g}_1(\boldsymbol{x}) = \begin{bmatrix} 0 \\ 0 \\ \frac{nRT}{V_1(x_1)} \\ 0 \end{bmatrix}, \quad \boldsymbol{g}_2(\boldsymbol{x}) = \begin{bmatrix} 0 \\ 0 \\ 0 \\ \frac{nRT}{V_2(x_1)} \end{bmatrix}. \tag{15}$$

As candidates for the components of a flat output $\boldsymbol{z} = \boldsymbol{h}(\boldsymbol{x})$ of the system we choose the angle $z_1 = x_1$ and the mean pressure $z_2 = (x_3 + x_4)/2$, and verify them in the following.

The concept of differential flatness is closely related to exact feedback linearization. If a system is feedback linearizable by static feedback with respect to a certain output, then the system is differentially flat with respect to that output [13]. The exact linearization problem in turn is solvable if and only if the system has the vector relative degree $\{\rho_1, \rho_2\}$ and $\sum_i^m \rho_i = n$ [12]. A two-input two-output nonlinear system of the form (13) has a relative degree $\{\rho_1, \rho_2\}$ at a point $\boldsymbol{x}_0$ if the following conditions in terms of Lie deriviatives hold (cf. [12]):

1) $L_{\boldsymbol{g}_j} L_{\boldsymbol{f}}^k \boldsymbol{h}_i(\boldsymbol{x}) = 0$ for all $1 \leq i, j \leq 2$, for all $k < \rho_i - 1$, for all $\boldsymbol{x}$ in a neighborhood of $\boldsymbol{x}_0$.
2) The matrix

$$\boldsymbol{\kappa}(\boldsymbol{x}) = \begin{bmatrix} L_{\boldsymbol{g}_1} L_{\boldsymbol{f}}^{\rho_1 - 1}\boldsymbol{h}_1(\boldsymbol{x}) & L_{\boldsymbol{g}_2} L_{\boldsymbol{f}}^{\rho_1 - 1}\boldsymbol{h}_1(\boldsymbol{x}) \\ L_{\boldsymbol{g}_1} L_{\boldsymbol{f}}^{\rho_2 - 1}\boldsymbol{h}_2(\boldsymbol{x}) & L_{\boldsymbol{g}_2} L_{\boldsymbol{f}}^{\rho_2 - 1}\boldsymbol{h}_2(\boldsymbol{x}) \end{bmatrix}, \tag{16}$$

is nonsingular at $\boldsymbol{x} = \boldsymbol{x}_0$.

By computation of the respective Lie derivatives of the system (14),(15), we find for all $\boldsymbol{x}$ that $\rho_1 = 3$ and $\rho_2 = 1$, whose sum is equal to n. Beyond that, the coupling matrix $\boldsymbol{\kappa}(\boldsymbol{x})$ is nonsingular for all $\boldsymbol{x}$. Therefore, the system is differentially flat.

Based thereon, a static input transformation which achieves an I/O linearization and decoupling of the nonlinear system (14),(15) is given by

$$\boldsymbol{u}(\boldsymbol{x}) = \boldsymbol{\kappa}^{-1}(\boldsymbol{x})\ (\boldsymbol{\nu} - \boldsymbol{a}(\boldsymbol{x}))\,. \tag{17}$$

with compensation term

$$\boldsymbol{a}(\boldsymbol{x}) = \begin{bmatrix} L_{\boldsymbol{f}}^3 \boldsymbol{h}_1(\boldsymbol{x}) \\ L_{\boldsymbol{f}} \boldsymbol{h}_2(\boldsymbol{x}) \end{bmatrix} \tag{18}$$

and new input $\boldsymbol{\nu}$. We employ feedback linearization with $\boldsymbol{x}$ in (17) being the measured state, which is evidently

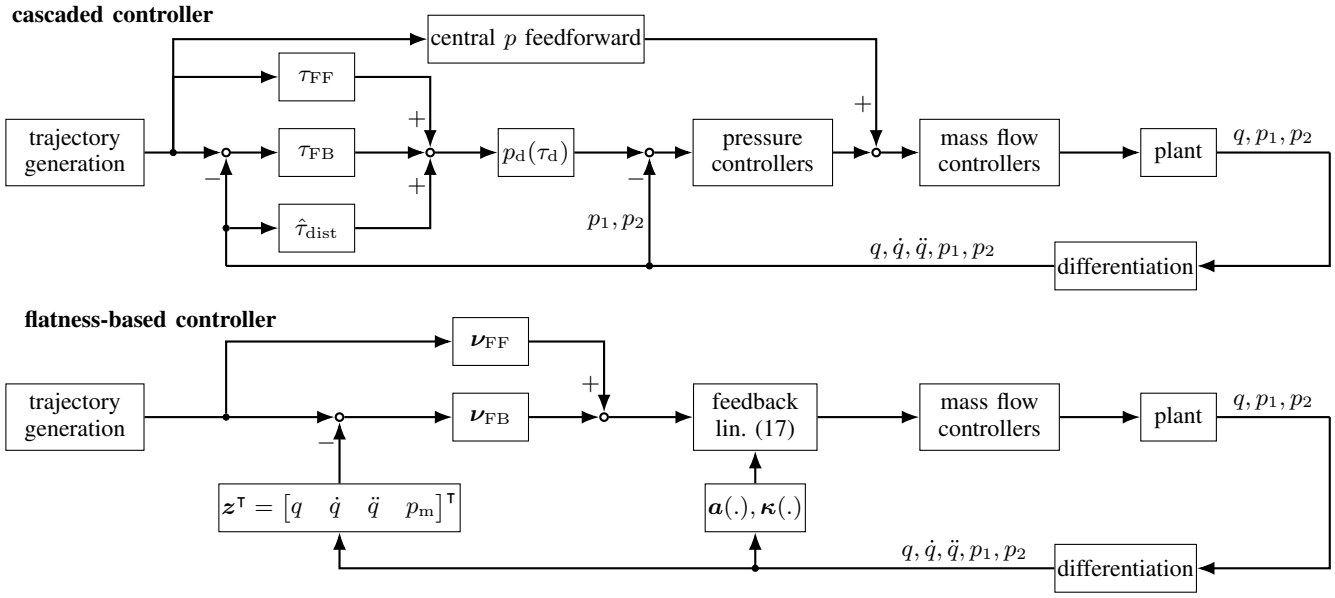

Fig. 2. Top: Cascaded control structure. Bottom: Flatness-based control structure.

more robust than just feedforward linearization that is often applied in the field. The vector $\boldsymbol{a}(\boldsymbol{x})$ contains model-based friction compensation, because τ_{f} from (14) is also included in the Lie derivative in (18).

For the two resulting decoupled integrator chains, we design linear controllers

$$\begin{aligned} \nu_1 &= \dddot{z}_{1,\mathrm{d}} + c_{1,2}(\ddot{z}_{1,\mathrm{d}} - \ddot{z}_1) + c_{1,1}(\dot{z}_{1,\mathrm{d}} - \dot{z}_1) + c_{1,0}(z_{1,\mathrm{d}} - z_1) \\ \nu_2 &= \dot{z}_{2,\mathrm{d}} + c_{2,0}(z_{2,\mathrm{d}} - z_2) \end{aligned} \tag{19}$$

for output tracking $z_i(t) \to z_{i,\mathrm{d}}(t)$, comprised of stabilizing feedback and feedforward. The corresponding error dynamics read

$$\begin{aligned} \dddot{e}_1 + c_{1,2}\ddot{e}_1 + c_{1,1}\dot{e}_1 + c_{1,0}e_1 &= 0 \\ \dot{e}_2 + c_{2,0}e_2 &= 0 \end{aligned} \tag{20}$$

We choose the dynamics of the trajectory tracking error e_1 as a series interconnection of a PT_2 and PT_1 system with identical corner frequency. As an alternative, the linear controllers (19) for the integrator chains are designed via LQR. This leads to comparable results, so that in the following the first mentioned, physically interpretable design is preferred.

The above feedback control law requires the first and second derivative of the joint angle. In the experiment, these are obtained by a real differentiator, by means of feasible encoder accuracy. Alternatively, the acceleration is reconstructed model-based in an observer, which in experiments, for the present hardware, reduces noise but makes the system more susceptible to model errors such as payload variations or unmodeled frictional effects. With robustness being favored, in the following the signal from real differentiation is fed back into the overall closed loop system.

The flatness-based controller scheme is depicted in Fig. 2.

IV. EXPERIMENTAL RESULTS

The experiments are carried out using a dSPACE rapid prototyping system with the controllers running at 1 kHz. Both the flatness-based controller and the outer loop of the cascaded controller are tuned with a corner frequency of 5 Hz. The pressure controller in the cascaded structure is tuned at 30 Hz, which is sufficiently faster than the outer loop, and provides a compromise between performance and robustness towards measurement noise. We choose the mean pressure 3.5 bar, allowing a wide range of pressure differences for generating the actuation torque. We investigate the tracking of feasible C^3 trajectories that cover the whole angular range of the joint.

In a first set of measurements, we examine the impact of the DOB on the cascaded controller. Fig. 3 shows the joint angle and corresponding tracking error without and with DOB. Tracking errors occur in both setups at the beginning of a transition, when unmodeled effects like stick-slip or varying friction parameters emerge, such that friction feedforward τ_{f} can never be exact. The DOB improves trajectory tracking significantly. With the observer's underlying integrator model, stationary errors are reduced, whereas without DOB a stationary error persists. Still, at some points, stick-slip occurs, which could for example be addressed with gain scheduling of the integral part.

Next, we compare the performance of the cascaded and the flatness-based controller, both tuned as similar as possible, as stated at the beginning of this section. Both controllers' trajectory tracking behavior and corresponding error is shown in Fig. 4. The tracking error of the flatness-based controller is smaller than the one of the cascaded controller. Quantitatively, the root-mean-square error over the course of the trajectory is reduced by 48.0 %. The first main difference is the flatness-based controller's smaller error at the beginning

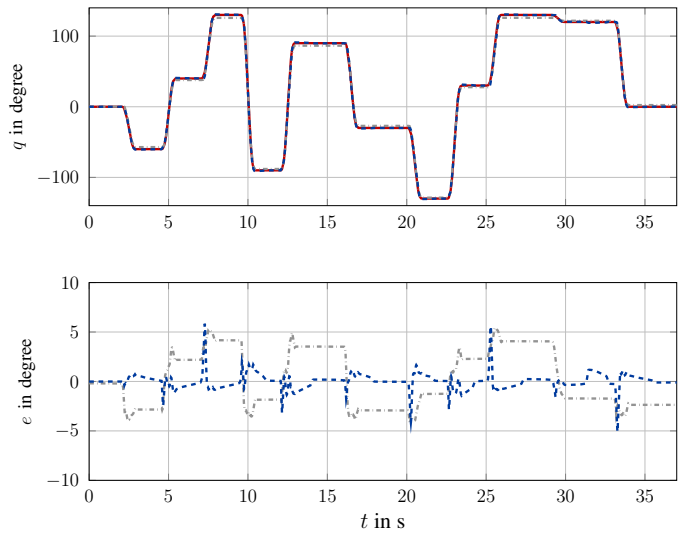

Fig. 3. Top: Desired and acutal joint angle. Bottom: Tracking error. Reference trajectory —, without DOB – –, with DOB –·–·–.

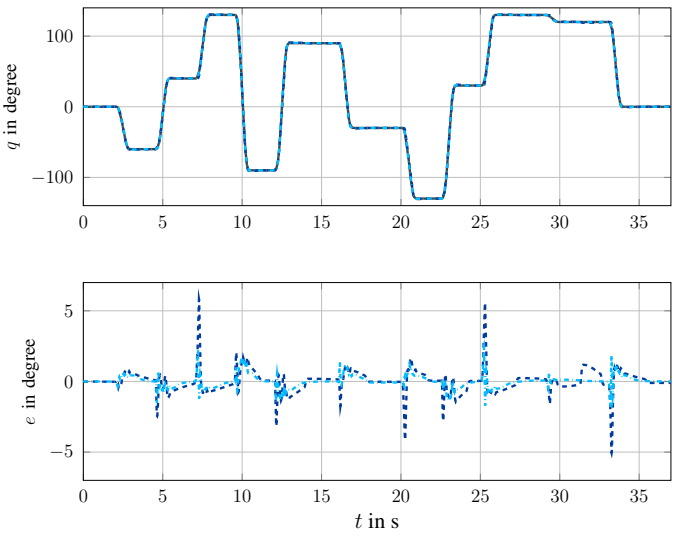

Fig. 4. Top: Desired and acutal joint angle. Bottom: Tracking error. Reference trajectory —, cascaded controller – –, flatness-based controller –·–·–.

of setpoint transitions. The reason for this is that, in contrast to the cascaded controller, the flatness-based controller (19) does not only contain the position and velocity error, but also the acceleration error. The latter is on the same differential level as the friction torque, so that friction disturbances are compensated directly by this feedback. In the cascaded controller, such disturbance torque has to be captured by the DOB first, and only then the required pressure difference to overcome it is set by the inner control loop. The acceleration gain in the flatness-based controller should not be tuned too aggressively though, in order to avoid a too dominant feedback of oscillations, which may occur. Another reason is that the feedback in the flatness-based controller has a direct feedthrough to the pressure dynamics, and is not just acting on the desired torque. Therefore, it is able to react faster, given the physically constrained pressure dynamics.

Second, the two controllers show different behavior when bringing the joint to a halt at the end of a transition. This results from the structural difference in how the controllers deal with friction. The cascaded controller applies (2) as feedforward in the torque domain. The flatness-based controller, however, is implemented in the mass flow domain. Therefore, it requires the derivative of (2), which is $1/\left(\dot{q}_c \cosh^2\left(\frac{\dot{q}}{\dot{q}_c}\right)\right)$, generating a mass flow peak as friction feedforward control. This mass flow peak is applied at the beginning of a transition for the joint to break loose. For braking towards standstill, however, mass flow domain friction feedforward is turned off. This becomes necessary, because the smooth approximation of Coulomb friction with a $\tanh$ function and its derivative already compensate for friction before $\dot{q} = 0$ is reached during braking, which leads to a mass flow peak causing overshoot in the experiment. With the flatness-based controller, reaching the target angle is therefore mostly achieved by feedback. With the cascaded controller in contrast, the friction feedforward torque ends,

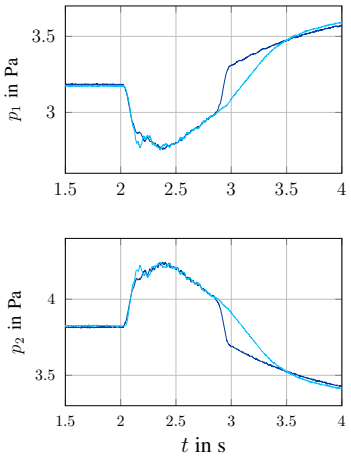

Fig. 5. Experimental pressures during one transition: cascaded controller —, flatness-based controller —.

which leads to a visible drop in pressure difference. This effect is shown in Fig. 5 at $t = 2.9\ s$ for one exemplary transition, whereas the flatness-based controller drives the joint more steadily. The DOB then starts to estimate a disturbance torque, which is saturated by model-based design as described before, and may not able to overcome static friction, once the drive is in standstill, because the resulting desired pressure difference may be too low.

In order to evaluate the controllers' robustness, we attach an additional mass of 1 kg to the actuator as a payload disturbance. Both controllers are kept unchanged, i.e. only the flange of mass 100 g is considered in the model, and tuned with similar parameters for both control laws. The trajectory tracking results are depicted in Fig. 6, and show similar effects as in the previous case with the nominal payload.

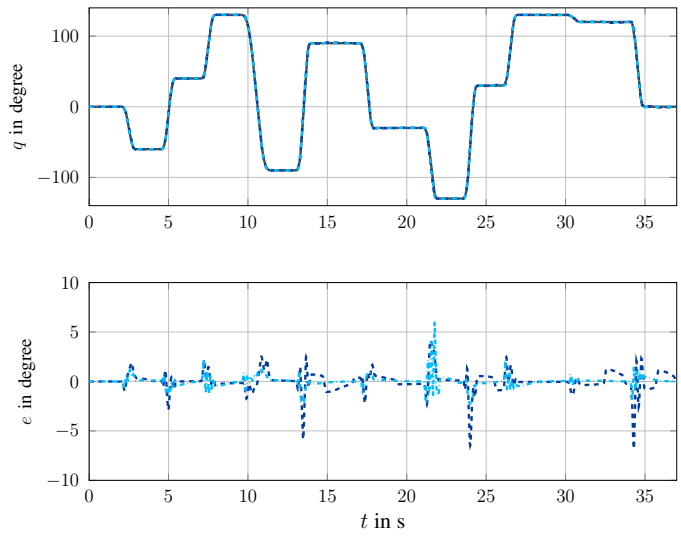

Fig. 6. Experimental trajectory tracking results with a 1 kg payload disturbance. Top: Desired and acutal joint angle. Bottom: Tracking error. Reference trajectory —, cascaded controller – –, flatness-based controller -·-·-.

First, the flatness-based controller reduces the maximum error, especially at the beginning of transitions. Second, it converges to the steady state faster. Despite the unmodeled load disturbance, both controllers still track the desired trajectory well. This is because both have a robustification towards disturbance torques, here resulting from payloads not taken into account in the model. In the flatness-based controller, disturbance torques are compensated by acceleration feedback, in the cascaded controller by the torque DOB.

The two control approaches introduced in this work have some structural differences. By virtue of (17),(19) the flatness-based control mass flow is proportional to the tracking error. Hence, the controller has naturally integrating behavior with respect to the chamber pressure and, consequently, driving torque. In the cascaded controller, this can only be achieved by an additional integrator, preferably by a DOB with integral disturbance model.

As for the cascaded controller, first the outer loop controller, and in case of stationary errors the DOB, have to compute the desired torque. Then, the inner loop controller sets the desired pressures. The flatness-based controller, however, has direct feedthrough to the pressure dynamics, which enables a faster response. The acceleration feedback in the flatness-based controller turns out to be advantageous in the presence of friction effects, which occur especially towards the beginning and end of transitions.

When it comes to the feedback into both controllers, the cascaded controller requires the measured signals q and $\dot{q}$, whereas the flatness-based controller (19) requires one more derivative, up to $\ddot{q}$. That is why the quality of the acceleration signal is crucial. Both a real differentiator and an observer can induce phase delay as well as noise, so that they have to be tuned carefully. In the above experiments, a real differentiator is used, which is possible due to a high encoder accuracy.

V. CONCLUSION

In this work, a pneumatically-driven rotary joint was introduced and controlled with two different model-based nonlinear control laws. These were, first, a cascaded controller and DOB with integrating behavior, and second, a flatness-based controller. It was demonstrated experimentally that both controllers track reference trajectories well. In the light of these measurements, the differences between the control structures and the resulting trajectory tracking behavior were analyzed. Also with an unmodeled payload disturbance, both controllers performed well, because they include structural properties that enhance robustness.

This work, dealing with a single joint, provides the foundation for the control of more involved robots with pneumatic rotary joints. Cascaded control has already been applied by researchers to several other types of robotic manipulators. In this work, the flatness-based controller achieved a better performance than the cascaded controller. Thus, it is desirable to extend this concept to entire robots with pneumatic drives. For coupled manipulator structures, this will, however, be computationally more complex than cascaded control.

REFERENCES

[1] B. Tondu, "Modelling of the McKibben artificial muscle: A review," *Journal of Intelligent Material Systems and Structures*, vol. 23, no. 3, pp. 225–253, 2012.

[2] B. Rouzbeh, G. M. Bone, and G. Ashby, "High-accuracy position control of a rotary pneumatic actuator," *IEEE/ASME Transactions on Mechatronics*, vol. 23, no. 6, pp. 2774–2781, 2018.

[3] J. Fras, Y. Noh, H. Wurdemann, and K. Althoefer, "Soft fluidic rotary actuator with improved actuation properties," in *2017 IEEE/RSJ International Conference on Intelligent Robots and Systems (IROS)*. IEEE, 2017.

[4] E. Richer and Y. Hurmuzlu, "A high performance pneumatic force actuator system: Part I—nonlinear mathematical model," *Journal of Dynamic Systems, Measurement, and Control*, vol. 122, no. 3, pp. 416–425, 2000.

[5] X. Brun, M. Belgharbi, S. Sesmat, D. Thomasset, and S. Scavarda, "Control of an electropneumatic actuator: comparison between some linear and non-linear control laws," *Proceedings of the Institution of Mechanical Engineers, Part I: Journal of Systems and Control Engineering*, vol. 213, no. 5, pp. 387–406, 1999.

[6] M. Göttert and R. Neumann, "Bahnregelung servopneumatischer Antriebe – ein Vergleich von linearen und nichtlinearen Reglern (Continuous path control of servo pneumatic drives – a comparison of linear and nonlinear controllers)," *at – Automatisierungstechnik*, vol. 55, no. 2, 2007.

[7] A. Hildebrandt, O. Sawodny, R. Neumann, and A. Hartmann, "A cascaded tracking control concept for pneumatic muscle actuators," in *2003 European Control Conference (ECC)*. IEEE, 2003, pp. 2517–2522.

[8] A. Raisch, A. Mayer, D. Müller, A. Hildebrandt, and O. Sawodny, "A model-based cascaded control concept for the bionic motion robot," in *2020 American Control Conference (ACC)*. IEEE, 2020, pp. 2049–2054.

[9] M. Göttert, "Bahnregelung servopneumatischer Antriebe," Ph.D. dissertation, Universität Siegen, 2003.

[10] ISO, "International Organization for Standardization: ISO 6358-1:2013 Pneumatic fluid power – determination of flow-rate characteristics of components using compressible fluids," 2013.

[11] M. W. Spong, S. Hutchinson, and M. Vidyasagar, *Robot modeling and control*. Hoboken, N.J.: Wiley, 2006.

[12] A. Isidori, *Nonlinear control systems*, 3rd ed., ser. Communications and control engineering series. London: Springer, 1995.

[13] R. Rothfuß, *Anwendung der flachheitsbasierten Analyse und Regelung nichtlinearer Mehrgrößensysteme*, ser. Fortschrittberichte VDI Reihe 8, Meß-, Steuerungs- und Regelungstechnik. Düsseldorf: VDI-Verl., 1997, vol. Nr. 664.